

# Few-shot Action Recognition with Implicit Temporal Alignment and Pair Similarity Optimization

Congqi Cao<sup>a,b,\*\*</sup>, Yajuan Li<sup>a,c</sup>, Qinyi Lv<sup>d</sup>, Peng Wang<sup>a,b</sup>, Yanning Zhang<sup>a,b</sup>

<sup>a</sup>National Engineering Laboratory for Integrated Aero-Space-Ground-Ocean Big Data Application Technology, Northwestern Polytechnical University, Xi'an 710129, China

<sup>b</sup>School of Computer Science, Northwestern Polytechnical University, Xi'an 710129, China

<sup>c</sup>School of Cybersecurity, Northwestern Polytechnical University, Xi'an 710129, China

<sup>d</sup>School of Electronics and Information, Northwestern Polytechnical University, Xi'an 710129, China

---

## ABSTRACT

Few-shot learning aims to recognize instances from novel classes with few labeled samples, which has great value in research and application. Although there has been a lot of work in this area recently, most of the existing work is based on image classification tasks. Video-based few-shot action recognition has not been explored well and remains challenging: 1) the differences of implementation details among different papers make a fair comparison difficult; 2) the wide variations and misalignment of temporal sequences make the video-level similarity comparison difficult; 3) the scarcity of labeled data makes the optimization difficult. To solve these problems, this paper presents 1) a specific setting to evaluate the performance of few-shot action recognition algorithms; 2) an implicit sequence-alignment algorithm for better video-level similarity comparison; 3) an advanced loss for few-shot learning to optimize pair similarity with limited data. Specifically, we propose a novel few-shot action recognition framework that uses long short-term memory following 3D convolutional layers for sequence modeling and alignment. Circle loss is introduced to maximize the within-class similarity and minimize the between-class similarity flexibly towards a more definite convergence target. Instead of using random or ambiguous experimental settings, we set a concrete criterion analogous to the standard image-based few-shot learning setting for few-shot action recognition evaluation. Extensive experiments on two datasets demonstrate the effectiveness of our proposed method.

---

*Keywords:* Few-shot action recognition; Temporal modeling; Implicit alignment; Similarity optimization

## 1. Introduction

Few-shot action recognition aims to recognize novel actions with only a few labeled samples. It has a wide application in practical scenarios since labeling videos is expensive and there is a demand for task-specific or user-defined action recognition. However, insufficient annotated data makes the current popular and successful deep learning-based algorithms hard to learn patterns and optimize.

Like the image-based few-shot object classification task that has been widely studied recently (Sung et al., 2018; Chen et al., 2019; Finn et al., 2017; Li et al., 2019a; Xian et al., 2019; Zhang et al., 2019), the solutions for video-based few-shot action recognition fall into three categories: 1) metric learning by comparing the similarity between the unknown data and the labeled samples (Tan and Yang, 2019; Bishay et al., 2019; Cao et al., 2020); 2) fast adaptation by learning an optimal initialization status to train a classifier (Coskun et al., 2019); 3) data augmentation by generating additional training data (Kumar Dwivedi et al., 2019). The last kind of solution still needs to learn a metric or train a classifier for unlabeled data recognition. The first and the second kinds of solution can be seen as learning with pair-wise labels and learning with class-level labels respectively. As analyzed in Sun et al. (2020), learning with class-level labels also calculates the similarity scores between samples and a set of proxies (*i.e.*, classification weight

---

\*\*Corresponding author:

*e-mail:* congqi.cao@nwpu.edu.cn (Congqi Cao)

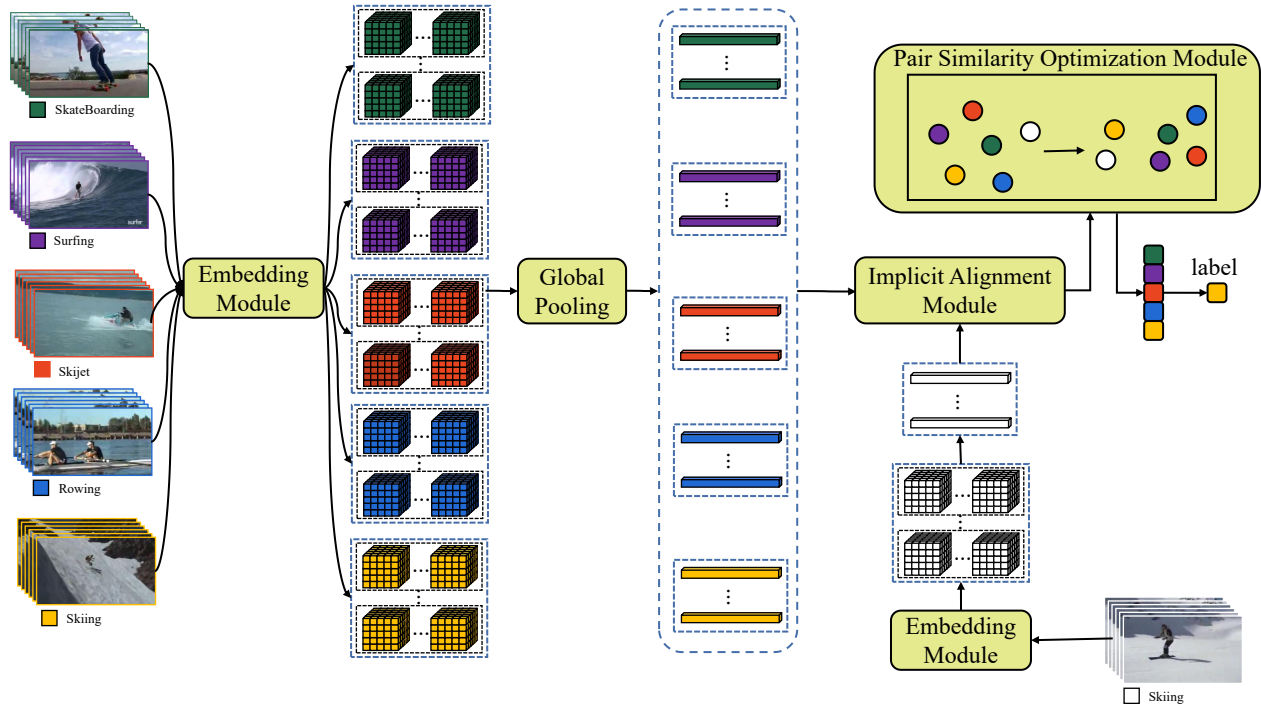


**Fig. 1** . Overview of our model for few-shot action recognition in 5-way 1-shot setting. As shown, this framework consists of an embedding module, an implicit alignment module and a pair similarity optimization module. We first extract the local spatiotemporal features with the embedding module. And then the implicit alignment module is used to align a given query video with the support videos semantically at video-level. Finally, we use the pair similarity optimization module to optimize pair similarity.

vectors) representing each class. Therefore, these two learning approaches can be unified in a pair similarity optimization perspective, which aims to maximize the within-class similarity and minimize the between-class similarity.

However, it is challenging to compare and measure the similarity between videos for few-shot action recognition. Few-shot action recognition not only faces the difficulty of data scarcity and semantic misalignment in appearance as image-based few-shot object classification does, but also needs to solve the problem of long-term temporal modeling and learning a distance measurement to compare sequences. On images, the deformation and arbitrary location of objects may cause ambiguity when comparing two images directly. To address this issue, Hao et al. (2019) calculate the similarity of each local region pairs of the feature maps extracted from the query image to be classified and the support images with labels to find the potential semantically relevant pairs for comparison. Li et al. (2019b) conduct a local descriptor based measure via k-nearest neighbor search over the deep local descriptors. Lifchitz et al. (2019) perform dense classification over feature maps to take full advantage of the local activations. For action recognition, due to the additional temporal dimension, there are wide variations and enormous information in video. Directly comparing the similarity of each local region pairs in the spatiotemporal space will take a huge computation cost. Besides that, the neglect of temporal ordering information is unfavorable for action recognition since temporal information plays an important role. To

leverage the temporal information in video data, Tan and Yang (2019) encode videos as dynamic images (Bilen et al., 2016) and use a CNN to get an incorporating feature for similarity learning. Bishay et al. (2019) utilize a segment-by-segment attention mechanism to perform temporal alignment. Cao et al. (2020) explicitly align video sequences with a variant of the Dynamic Time Warping (DTW) algorithm (Müller, 2007). However, the routines of actions are generally not fixed since performers can change their habits, *i.e.*, the location and duration of each atomic step can vary drastically, even some atomic steps can be omitted. It is difficult to align two appearance-different sequences explicitly, especially with scarce labeled data for training. Thus, in this paper, we propose to align video sequences implicitly and optimize video-level pair similarity directly for few-shot action recognition.

In concrete, we propose to use long short-term memory (LSTM) (Hochreiter and Schmidhuber, 1997) following 3D convolutional embedding layers (Chen et al., 2018) for sequence modeling. Instead of calculating the similarity between segment-level features, we measure the distance between video-level descriptors for semantic alignment and comparison. To alleviate the optimization challenge caused by extremely limited annotated data and find a better convergence status with a more flexible process, we adopt circle loss (Sun et al., 2020), which re-weights each similarity to highlight the less-optimized ones instead of using an equal penalty, for pair similarity optimization. The framework of our proposed model is illustrated

in Fig. 1. We design extensive experiments to evaluate the performance of our method. Nevertheless, another outstanding issue of few-shot action recognition is lack of standard and unambiguous settings for performance evaluation. The existing work randomly divides the datasets into training, validation and test splits with different ratios (Zhu and Yang, 2018; Kumar Dwivedi et al., 2019; Tan and Yang, 2019; Cao et al., 2020; Bishay et al., 2019; Bo et al., 2020; Zhang et al., 2020). Even some work does not set a validation set. The number of samples selected for each training episode is inconsistent. And the accuracies are computed by averaging over different numbers of episodes generated randomly from the test split. To make a fair comparison with competing methods, we establish a specific and clear experimental setting on UCF101 and HMDB51 datasets, which can be used as a standard setting for few-shot action recognition evaluation.

In summary, our main contributions include:

- We propose a novel few-shot action recognition model to compare video sequences with implicit alignment and long-term temporal modeling.
- We propose to re-weight the video-level similarity scores depending on their status flexibly during training, which benefits the optimization process.
- Extensive experiments are conducted with a clearly defined experimental setting that can be seen as a standard evaluation criterion for few-shot action recognition. The proposed method outperforms competing methods by 13%-17% in 5-way 1-shot learning and 10%-12% in 5-way 5-shot learning.

## 2. Related Work

**Few-shot learning.** Few-shot learning has attracted increasing attention recently, especially on the image-based classification task. Current work on this task can be roughly divided into three categories: (i) metric learning-based methods, (ii) fast adaptation-based methods, and (iii) data augmentation-based methods.

The metric learning-based methods aim to learn an embedding space and a corresponding metric function to measure the similarity or distance between samples, by which intra-class samples are closer while inter-class samples are farther away (Koch et al., 2015; Snell et al., 2017). For better metric learning ability, Sung et al. (2018) present a learnable relation module to compute the similarity score. Oreshkin et al. (2018) propose a task dependent adaptive metric. Huang et al. (2019) use pairwise bilinear pooling for feature comparison. To alleviate the problem of object deformation and misalignment, Hao et al. (2019) calculate the similarity scores of local region pairs and re-weight these local scores to obtain the image-level similarity. Li et al. (2019b) conduct k-nearest search over the local descriptors to replace the image feature based measure by a local descriptor based measure. However, as the feature space increases, extra computational cost and parameters are introduced. The fast adaptation-based methods aim

to learn a good initialization or update strategy of a learner so that the learner can quickly adapt to new tasks. Ravi and Larochelle (2017) train an LSTM-based meta-learner model to learn both a good initialization and a parameter updating mechanism for the learner network. Finn et al. (2017) propose to find an initialization that can be quickly adapted to a new task via a few gradient steps. Instead of sharing an initialization between tasks forcibly, Baik et al. (2020) propose a task-dependent layer-wise attenuation to dynamically control how much of prior knowledge each layer would exploit for a given task. The main problem of this kind of methods is the difficulty in applying to domains with large gap and tasks with conflicts. Data augmentation-based methods generally supplement training samples by generative models or make full use of data characteristics through self-supervised and unsupervised learning methods (Xian et al., 2019; Zhang et al., 2019; Gidaris et al., 2019). However, this kind of methods does not solve the issue that the learning algorithms heavily depend on a large number of training samples.

**Few-shot action recognition.** Few-shot action recognition is a branch of few-shot learning that based on video. Besides the spatial appearance, temporal motion information plays an important role for few-shot action recognition.

In the metric learning paradigm, Guo et al. (2018) propose Neural Graph Matching (NGM) Network, which jointly learns a graph generator and a graph matching metric function, for 3D few-shot learning action recognition. NGM uses graphical structure to model the spatial relationship and to capture the temporal evolution of videos. Tan and Yang (2019) condense videos into images with dynamic image (Bilen et al., 2016), then use a CNN to get an incorporating feature and learn a similarity metric of it. Bo et al. (2020) propose Temporal Attention Vectors (TAVs) to encode the video-wide temporal information by calculating the weighted sum of all frame features. Temporal Attentive Relation Network (TARN) (Bishay et al., 2019) utilizes a segment-by-segment attention mechanism for temporal alignment and learns a distance measure on the aligned representations. Cao et al. (2020) propose to use a variant of the Dynamic Time Warping (DTW) algorithm (Müller, 2007) to align and measure the distance between videos. However, aligning the semantic content in videos is still challenging since there are wide variations and the data is extremely limited. In the fast adaptation paradigm, Zhu and Yang (2018) introduce a multi-saliency algorithm to encode videos into matrix representations and use a compound memory network for classification. Coskun et al. (2019) develop a low-shot transfer learning method to learn domain invariant features for first-person action recognition. In the augmentation paradigm, Kumar Dwivedi et al. (2019) propose ProtoGAN which is a conditional generative adversarial network to synthesize additional examples for novel categories. Zhang et al. (2020) use spatial and temporal attention modules to localize actions and enrich the training data by feeding numbers of augmented clips into the network with self-supervised loss. Generally, as the spatiotemporal modeling capacity of the model increases, the risk of overfitting also increases, since there are more parameters and few training data, which is a main problem of few-shot action recog-

nitition.

Another issue of few-shot action recognition is the lack of standard and unambiguous experimental settings for performance evaluation. The datasets are randomly divided into training, validation, and test splits with different ratios, even without the validation split (Kumar Dwivedi et al., 2019; Tan and Yang, 2019; Cao et al., 2020; Zhang et al., 2020). Besides that, the accuracies are computed by averaging over different numbers of episodes. On the other side, the experimental settings in image-based few-shot classification are clearly defined, including the data splits and the evaluation criterion.

**Similarity optimization.** The objective of few-shot learning can be seen as maximizing intra-class similarity as well as minimizing inter-class similarity (Bishay et al., 2019; Coskun et al., 2019; Cao et al., 2020). For metric learning-based methods, the similarity is calculated between samples. For fast adaptation-based methods with a classifier, the similarity is calculated between samples and the classification weight vectors. Thus, it is a pair similarity optimization problem.

Existing metric loss function (*e.g.* triplet loss (Hoffer and Ailon, 2015)) and classification loss function (*e.g.* softmax cross-entropy loss (Murphy, 2012)) impose an equal penalty on each similarity score, which is inflexible and non-optimal. Sun et al. (2020) propose to re-weight each similarity score to emphasize the less-optimized ones and verify the effectiveness of the proposed circle loss on face recognition, person re-identification, as well as fine-grained image retrieval tasks.

### 3. Proposed Method

Instead of aligning videos explicitly and rigidly as well as measuring similarity based on clip-level features (Bishay et al., 2019; Cao et al., 2020), which is non-optimal for long-term sequence modeling and hard to optimize since there are wide variations in video and the labeled data is extremely scarce, we propose a flexible video-level semantic alignment and similarity optimization mechanism for few-shot action recognition. The framework of our proposed model is shown in Fig. 1, which can be broadly divided into three major blocks: (a) an embedding module for spatiotemporal feature extraction, (b) an implicit alignment module to model long-term temporal information and align two sequences semantically in video-level, and (c) a pair similarity optimization module for adjusting gradients on similarity scores flexibly according to their optimization status. In the following, Section 3.1 describes the problem formulation of few-shot action recognition. Section 3.2, 3.3, 3.4 introduce the proposed modules in detail.

#### 3.1. Problem formulation

In few-shot action recognition setting, we divide the whole dataset into three sets: a training set  $N_{train}$ , a validation set  $N_{validation}$ , and a test set  $N_{test}$ . There is no overlapping category between the three sets. The training set has sufficient labeled data for each class, which minimizes the similarity loss over training episodes for few-shot learning. The validation set is used to select the optimal model. And the test set is used to

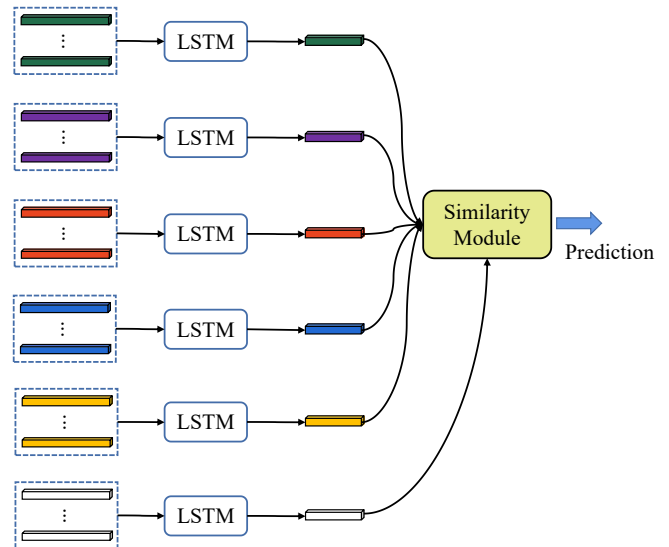


**Fig. 2.** Structure of the implicit alignment module. We use long short-term memory for sequence modeling and semantic alignment. Then, the similarity module is used to compare video-level similarities.

evaluate the performance *i.e.*, the accuracy is computed by averaging over a number of few-shot learning tasks sampled from the test set. For few-shot learning, the episode-based training method, which mimics few-shot learning tasks during training, proposed by Vinyals et al. (2016), is proved to be an effective training method. In the specific  $N$ -way  $K$ -shot few-shot learning task, each episode contains a support-set  $\mathcal{S}$  sampled from the training set  $N_{train}$ , which contains  $N \times K$  samples from  $N$  different classes where each class contains  $K$  support samples. Then  $Q$  samples from each class are selected to form the query set  $\mathcal{Q}$  which contains  $N \times Q$  samples. The goal is to classify the  $N \times Q$  query samples into  $N$  classes only with the  $N \times K$  support samples. In our setting, we give a specific number of the query set  $\mathcal{Q}$  in each episode, which is different from the earlier methods without a clearly defined value. Moreover, there is no standard for the division ratio of  $N_{train}$ ,  $N_{validation}$  and  $N_{test}$ . Some work even does not have  $N_{validation}$ . And the categories of  $N_{train}$ ,  $N_{validation}$  and  $N_{test}$  are randomly selected. However, the similarity between the categories in  $N_{train}$ ,  $N_{validation}$  and  $N_{test}$  has a strong influence on learning performance. We use an unambiguous and deterministic data splitting criterion in our paper to eliminate the influence of different divisions. In addition, the accuracies are computed by averaging over different numbers of episodes in the existing work. We give a specific and detailed evaluation setting in our experiments as a reference for subsequent work to make a fair comparison.

#### 3.2. Embedding Module

The embedding module  $f_\varphi$  generates the feature representations for the query and support videos, where  $f$  represents the projection function with learnable parameters  $\varphi$ . Discriminative spatiotemporal information is important while challenging to extract for few-shot action recognition with few labeled training

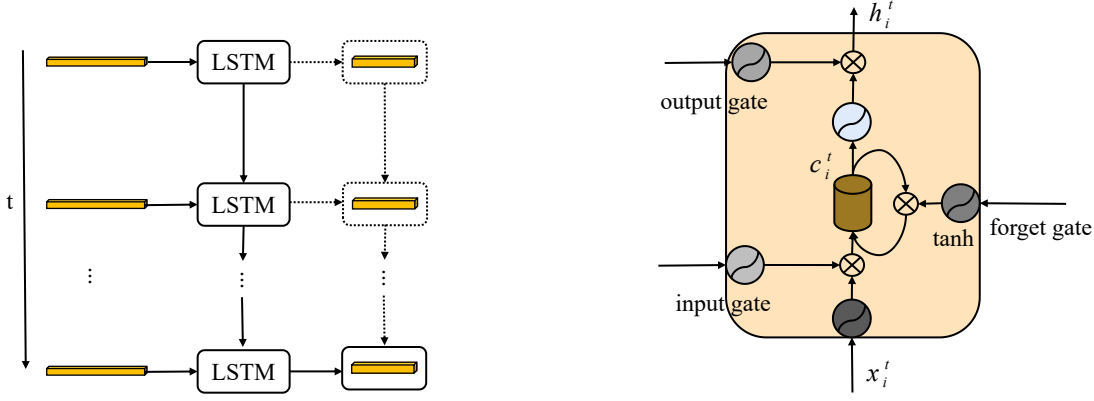


**Fig. 3.** Illustration of sequence modeling using the long short-term memory neural network between the video clips. The structure of LSTM is shown on the right.

data. Therefore, we choose to use a light-weight 3D convolutional neural network with good performance in action recognition to capture the spatiotemporal information. In our paper, the convolutional layers of the multi-fiber network (MFNet) (Kay et al., 2017) pre-trained on Kinetics-400 is selected as the embedding module  $f_\varphi$  to extract video features.

We divide a video into  $T$  clips. Each clip has a fixed number of frames. For an input video sequence  $x = \{x^1, x^2, \dots, x^T\}$ , we encode each clip  $x^t$  ( $t \in [1, \dots, T]$ ) with the embedding module into feature representation  $f_\varphi(x^t)$ , which makes  $f_\varphi(x)$  a set of feature vectors:

$$f_\varphi(x) = \{f_\varphi(x^1), f_\varphi(x^2), \dots, f_\varphi(x^T)\} \quad (1)$$

where the embedded feature dimension of each clip  $x^t$  is  $(C, T', H, W)$ . Specifically,  $C$  indicates the channel dimension,  $T'$  represents the temporal dimension,  $H$  and  $W$  are the height and width, respectively.

### 3.3. Implicit Alignment Module.

The implicit alignment module  $\mathcal{A}_\psi$  aims to model long-term temporal information and align two sequences semantically in the video-level. The structure of this module is illustrated in Fig. 2. First, we use long short-term memory for sequence modeling and implicit semantical alignment, as shown in Fig. 3. Next, the similarity module is used to optimize the video-level similarities.

In one episode, each support video  $x_i$  from the support set  $\mathcal{S} = \{(x_i, y_i)\}_{i=1}^G$  ( $G = N \times K, y_i \in \{1, \dots, N\}$ ), and the query video  $q$  from the query-set  $\mathcal{Q}$  are projected into the embedding feature space by the embedding module  $f_\varphi$ , which is followed by a dimensionality reduction function  $\mathcal{R}$  as the following equation:

$$\mathcal{R}(f(x_i)) = \{\mathcal{R}(f_\varphi(x_i^1)), \mathcal{R}(f_\varphi(x_i^2)), \dots, \mathcal{R}(f_\varphi(x_i^T))\} \quad (2)$$

where  $\mathcal{R}$  is a spatiotemporal dimension reduction function such as a global average/max pooling layer to prevent overfitting. We use global average pooling in our experiment.

Then, we use the long shot-term memory (LSTM) network to model the temporal relationship of the feature sequence  $(\mathcal{R}(f_\varphi(x_i^1)), \mathcal{R}(f_\varphi(x_i^2)), \dots, \mathcal{R}(f_\varphi(x_i^T)))$  and align two sequences

implicitly, as shown in Fig. 3. The LSTM computes the sequence of outputs  $(\mathcal{R}(f_\varphi(x_i^1)), \mathcal{R}(f_\varphi(x_i^2)), \dots, \mathcal{R}(f_\varphi(x_i^T)))$  by iterating the following equations:

$$I_i^t = \sigma(W_{xI}f_\varphi(\mathcal{R}(x_i^t)) + W_{hI}h_i^{t-1} + W_{cI} \circ c_i^{t-1} + b_I) \quad (3)$$

$$f_i^t = \sigma(W_{xf}f_\varphi(\mathcal{R}(x_i^t)) + W_{hf}h_i^{t-1} + W_{cf} \circ c_i^{t-1} + b_f) \quad (4)$$

$$c_i^t = f_i^t \circ c_i^{t-1} + I_i^t \circ \tanh(W_{xc}f_\varphi(\mathcal{R}(x_i^t)) + W_{hc}h_i^{t-1} + b_c) \quad (5)$$

$$o_i^t = \sigma(W_{xo}f_\varphi(\mathcal{R}(x_i^t)) + W_{ho}h_i^{t-1} + W_{co} \circ c_i^t + b_o) \quad (6)$$

$$h_i^t = o_i^t + \tanh(c_i^t) \quad (7)$$

where  $I_i^t, f_i^t, c_i^t, o_i^t, h_i^t$  indicate input gate, forget gate, cell status, output gate, hidden layer output respectively, and  $\circ$  denotes the Hadamard product, and  $t \in [1, T]$ . We use the output of the hidden layer  $h_i^t$  of the last time slice  $T$  as a video-level feature for  $x_i$ , which is denoted as  $\mathcal{A}_\psi(x_i)$ . For the query video  $q$  in each episode, we can get its video-level feature  $\mathcal{A}_\psi(q)$  as above.

Next, we calculate the similarity between the video-level features  $\mathcal{A}_\psi(x_i)$  and  $\mathcal{A}_\psi(q)$  by:

$$\cos(\mathcal{A}_\psi(x_i), \mathcal{A}_\psi(q)) = \frac{\mathcal{A}_\psi(x_i)^\top \mathcal{A}_\psi(q)}{\|\mathcal{A}_\psi(x_i)\| \cdot \|\mathcal{A}_\psi(q)\|} \quad (8)$$

where  $\cos(\cdot)$  indicates the cosine similarity whose value range is  $[-1, 1]$ , and  $\|\cdot\|$  means L2 norm. Other similarity or distance functions can also be employed.

The sequences are implicitly aligned by maximizing the similarity scores between the samples belonging to the same class and minimizing the similarity scores between the samples belonging to different classes during few-shot learning. For K-shot where  $K > 1$ , we average over the embedding features of all the samples from the same class to form a prototype feature of this class. The class probability of the query video is computed based on the similarity between the query video and the prototype features of all the classes.

### 3.4. Pair Similarity Optimization Module

Few-shot learning can be seen as maximizing intra-class similarity as well as minimizing inter-class similarity. Given a query video  $q$ , we calculate the similarity scores between  $q$

and the videos of the support set  $\mathcal{S}$  in each episode. For the negative sample from the inter-class, we denote its similarity score with the query video by  $s_n^j = \frac{\mathcal{A}_\psi(x_j)^\top \mathcal{A}_\psi(q)}{\|\mathcal{A}_\psi(x_j)^\top\| \cdot \|\mathcal{A}_\psi(q)\|}$  ( $x_j$  is the  $j$ -th sample in the negative sample set  $\mathcal{N}$  of the support set  $\mathcal{S}$ ). And for the positive sample from the intra-class, we denote its similarity score with the query video by  $s_p^i = \frac{\mathcal{A}_\psi(x_i)^\top \mathcal{A}_\psi(q)}{\|\mathcal{A}_\psi(x_i)^\top\| \cdot \|\mathcal{A}_\psi(q)\|}$  ( $x_i$  is the  $i$ -th sample in the positive sample set  $\mathcal{P}$  of the support set  $\mathcal{S}$ ). Maximizing the intra-class similarity as well as minimizing the inter-class similarity is equivalent to minimizing  $s_n - s_p$  by loss function:

$$\mathcal{L} = \log[1 + \sum_{i=1}^L \sum_{j=1}^M \exp(\gamma(s_n^j - s_p^i + m))] \quad (9)$$

where  $L = |\mathcal{P}|$ ,  $M = |\mathcal{N}|$ ,  $\gamma$  is a scale factor and  $m$  is a margin for better similarity separation.

However, the above method imposes an equal penalty on each similarity score, which is inflexible and non-optimal. Therefore, we follow recent work (Sun et al., 2020) to generalize  $s_n^j - s_p^i$  into  $\alpha_n^j s_n^j - \alpha_p^i s_p^i$ , which allows each similarity score to learn at its own pace. The loss function without margin is shown in Eq. 10. Note that  $\alpha_n$  and  $\alpha_p$  are independent weighting factors, allowing  $s_n$  and  $s_p$  to learn at different paces.

$$\begin{aligned} \mathcal{L}_{circle} &= \log[1 + \sum_{i=1}^L \sum_{j=1}^M \exp(\gamma(\alpha_n^j s_n^j - \alpha_p^i s_p^i))] \\ &= \log[1 + \sum_{j=1}^M \exp(\gamma \alpha_n^j s_n^j) \sum_{i=1}^L \exp(-\gamma \alpha_p^i s_p^i)] \end{aligned} \quad (10)$$

in which  $\alpha_n^j$  and  $\alpha_p^i$  are non-negative weighting factors.

Assume that the optimal value of  $s_p^i$  is  $O_p$  and the optimal value of  $s_n^j$  is  $O_n$ . When a similarity score deviates far from its optimum, it should get a large weighting factor so as to get effective update with large gradient. We follow Sun et al. (2020) to define  $\alpha_p^i$  and  $\alpha_n^j$  as follows:

$$\begin{cases} \alpha_p^i = [O_p - s_p^i]_+ \\ \alpha_n^j = [s_n^j - O_n]_+ \end{cases} \quad (11)$$

in which  $[\cdot]_+$  is the ‘‘cut-off at zero’’ operation to ensure  $\alpha_p^i$  and  $\alpha_n^j$  are non-negative.

Since  $s_n$  and  $s_p$  are in asymmetric position in Eq. 10. Naturally, it requires respective margins for  $s_n$  and  $s_p$ , which is formulated by:

$$\mathcal{L}_{circle} = \log[1 + \sum_{j=1}^M \exp(\gamma \alpha_n^j (s_n^j - \Delta_n)) \sum_{i=1}^L \exp(-\gamma \alpha_p^i (s_p^i - \Delta_p))] \quad (12)$$

in which  $\Delta_n$  and  $\Delta_p$  are the inter-class and intra-class margins, respectively.

Eq. 12 expects  $s_p^i > \Delta_p$  and  $s_n^j < \Delta_n$ . The setting of  $\Delta_p$  and  $\Delta_n$  can be analyzed by deriving the decision boundary. For simplicity, the case of binary classification is considered, in which the

decision boundary is achieved at  $\alpha_n(s_n - \Delta_n) - \alpha_p(s_p - \Delta_p) = 0$ . With Eq. 11 and Eq. 12, the decision boundary is formulated as:

$$(s_n - \frac{O_n + \Delta_n}{2})^2 + (s_p - \frac{O_p + \Delta_p}{2})^2 = C \quad (13)$$

in which  $C = ((O_n - \Delta_n)^2 + (O_p - \Delta_p)^2)/4$ . Eq. 13 shows that the decision boundary is the arc of a circle, so Eq. 12 is named circle loss.

There are five hyper-parameters for circle loss, *i.e.*,  $O_p$ ,  $O_n$  in Eq. 11 and  $\gamma$ ,  $\Delta_p$ ,  $\Delta_n$  in Eq. 12. The hyper parameters can be reduced by setting  $O_p = 1 + m$ ,  $O_n = -m$ ,  $\Delta_n = m$  and  $\Delta_p = 1 - m$ . Hence there are only two hyper-parameters, *i.e.*, the scale factor  $\gamma$  and the relaxation margin  $m$ .

The gradients of circle loss with respect to  $s_n^j$  and  $s_p^i$  are derived as follows:

$$\frac{\partial \mathcal{L}_{circle}}{\partial s_n^j} = Z \frac{\exp(\gamma((s_n^j)^2 - m^2))}{\sum_{l=1}^M \exp(\gamma((s_n^l)^2 - m^2))} \gamma(s_n^j + m) \quad (14)$$

and

$$\frac{\partial \mathcal{L}_{circle}}{\partial s_p^i} = Z \frac{\exp(\gamma(m^2 - (s_p^i - 1)^2))}{\sum_{k=1}^L \exp(\gamma(m^2 - (s_p^k - 1)^2))} \gamma(s_p^i - 1 - m) \quad (15)$$

in both of which  $Z = 1 - \exp(-\mathcal{L}_{circle})$

In our experiments, we verify the efficiency and effectiveness of re-weighting the similarity scores in the episode-based training stage. It is more flexible and can achieve better performance compared with traditional loss functions using equal penalty on each similarity score.

## 4. Experiments

In this section, we conduct comprehensive experiments to evaluate the proposed few-shot action recognition model and compare it with extensive baselines. The datasets used for evaluation are described in Section 4.1. Implementation details of the training and testing mechanism are described in Section 4.2. Detailed experimental results are described in section 4.3.

### 4.1. Datasets

We use two action recognition datasets to evaluate models, *i.e.*, the UCF101 dataset and the HMDB51 dataset.

**UCF101** (Soomro et al., 2012) is an action recognition dataset of realistic action videos collected from YouTube. There are 101 action categories and 13,320 videos. UCF101 is very challenging for few-shot action recognition which exists largest diversity in terms of actions and large variations in camera motion. For our experiments, we follow the splitting setting used by Zhang et al. (2020) which chooses 70, 10 and 21 non-overlapping classes for training, validation and testing, respectively. The specific action classes in the training split, validation split, and test split are listed in the supplementary material.

**HMDB51** (Kuehne et al., 2011) collects from various sources, mostly from movies, and a small proportion from public databases such as the Prelinger archive, YouTube and Google videos. It contains 6,849 videos divided into 51 action

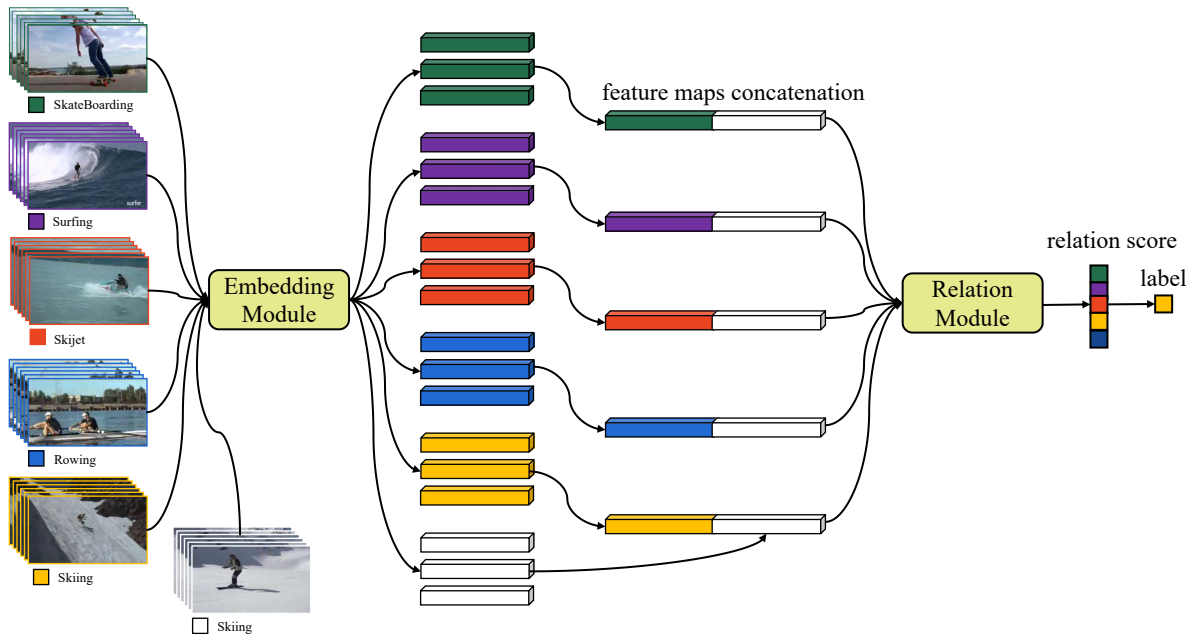


**Fig. 4.** Framework of the baseline Relation Video Network (RVN). It first extracts video features using the embedding module. Then the mean feature is computed as the centroid of each class. Next, the embedding features of the query video and each support video are concatenated. Finally, the relation module is used to compute the relation score between the query video and videos in the support set.

categories. Each category contains at least 101 videos. For our experiments, we follow the splitting setting used by Zhang et al. (2020) which chooses 31, 10 and 10 non-overlapping classes for training, validation, and testing, respectively. The specific action classes used for training, validation, and test are listed in the supplementary material.

#### 4.2. Implementation details

In an  $N$ -way  $K$ -shot task setting, we sample  $N \times K$  videos from  $N$  classes where each class has  $K$  examples as the support set. To be specific, 5-way 1-shot and 5-way 5-shot classification tasks are conducted on all datasets. During training, we sample 18,000 episodes to train our model. In each episode, we select  $N$  samples to build the query set, where each sample in the query set belongs to one of the  $N$  classes in the support set. During testing, we select 15 unlabeled samples from each class of  $N$  as the query set. Thus each testing episode has a total of  $N$  ( $K + 15$ ) examples. We sample 600 episodes from the test split in the experiments. This process is repeated ten times, and the final mean accuracy is reported. Moreover, the 95% confidence intervals are also reported. For both datasets, we divide each video into  $T$  segments, where  $T = 3$  in our experiment. In each segment, we uniformly sample 16 frames to form a clip. We use the input size of  $3 \times 16 \times 112 \times 112$  for training and testing. Here 3, 16, and  $112 \times 112$  are the channel dimension, the number of frames for each input clip and the spatial resolution of each frame, respectively. We follow the video preprocessing procedure in multi-fiber network (MFNet) (Chen et al., 2018). During training, we first resize the frames in the sampled clip to  $256 \times 256$  and then randomly crop a  $112 \times 112$  area. In the inference phase, we change the random crop to center crop. We ap-

ply stochastic gradient descent (Bottou, 2010) to optimize our model during the episode-based few-shot learning stage, with an initial learning rate of 0.00001 and decaying every 12,000 episodes by 0.1. All experiments are conducted using PyTorch (Paszke et al., 2017).

#### 4.3. Experimental Results

In this section, we first describe the architecture of baseline model in Section 4.3.1. Then, we presents ablation studies in Section 4.3.2. We report the results of our proposed framework compared with other methods in Section 4.3.3. Finally, we visualize the similarity matrices in Section 4.3.4.

##### 4.3.1. Baseline model

To verify the importance of modeling spatiotemporal relationships, we design a baseline architecture, Relation Video Network (RVN). Our baseline model RVN consists of two modules: an embedding module  $f_\varphi$  and a relation module  $g_\phi$ , as shown in Fig. 4.

In each episode, the support video  $x_i$  from the support-set  $\mathcal{S}$  and the query video  $q$  from the query-set  $\mathcal{Q}$  are fed into the embedding module  $f_\varphi$ , which generates the embedding feature maps  $f_\varphi(x_i) = \{f_\varphi(x_i^1), f_\varphi(x_i^2), \dots, f_\varphi(x_i^T)\}$  and  $f_\varphi(q) = \{f_\varphi(q^1), f_\varphi(q^2), \dots, f_\varphi(q^T)\}$ , respectively. The video-level features of the support video and the query video are obtained by averaging over the  $T$  clip-level feature maps, which are denoted as  $\mathcal{M}(f_\varphi(x_i))$  and  $\mathcal{M}(f_\varphi(q))$ , respectively, where  $\mathcal{M}$  represents the mean operation. Then, the video-level features are concatenated by the operator of  $C(\mathcal{M}(f_\varphi(x_i)), \mathcal{M}(f_\varphi(q)))$ . Subsequently, the combined feature of the support video and query

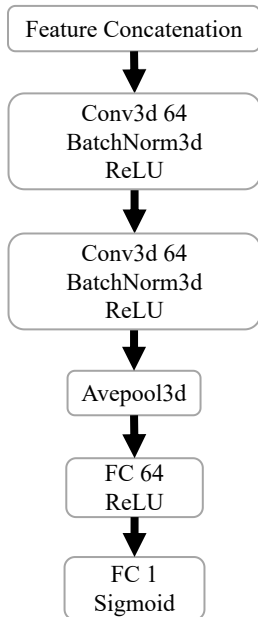


**Fig. 5** Structure of the relation module in RVN.

**Table 1**

The 5-way 1-shot accuracy results of different structures of the relation module on UCF101 dataset. The second column indicates the size of the convolution kernels used by the relation module in RVN.

Model	Convolution kernel	Accuracy (%)
RVN-1	$3 \times 3 \times 3, 3 \times 3 \times 3$	<b><math>80.33 \pm 0.25</math></b>
RVN-2	$3 \times 3 \times 3, 3 \times 1 \times 1$	$77.83 \pm 0.26$
RVN-3	$1 \times 3 \times 3, 1 \times 3 \times 3$	$76.87 \pm 0.27$

video is fed into a relation module  $g_\phi$ , which generates a relation score between 0-1 to indicate the similarity of the support video  $x_i$  and the query video  $q$ . The structure of the relation module  $g_\phi$  is shown in Fig. 5. Specifically, it mainly contains two convolution layers, a global average pooling layer, and two fully-connected layers. Each convolution layer is composed of a 3D convolution with 64 filters, a batch normalization and a ReLU activation. The dimensions of the two fully-connected layers are 64 and 1, respectively. Finally, a sigmoid activation is used to obtain the relation score in  $[0, 1]$  range.

#### 4.3.2. Ablation Studies

Here we perform ablation experiments to verify the effectiveness of modeling spatiotemporal relationships, verify the importance of long-term temporal modeling and explore the impact of circle loss. The default setting is 5-way 1-shot learning.

**Influence of relation.** To verify the effectiveness of modeling spatiotemporal relationships, we perform an ablation study by developing three different relation modules and analyzing the effects of different relation modules. Specifically, the first relation module named RVN-1 uses  $3 \times 3 \times 3$  convolutional kernels in both convolution layers. As for the second relation

**Table 2**

The 5-way 1-shot accuracy results of different LSTM structures on UCF101 dataset.

Units in hidden layer	Accuracy (%)
512	<b><math>86.57 \pm 0.21</math></b>
256	$85.14 \pm 0.22$
64	$74.74 \pm 0.25$

**Table 3**

Evaluation of cross-entropy loss and circle loss. We report the 5-way 1-shot on UCF101 dataset.

Model	Loss Function	Accuracy (%)
Our method	Circle loss	<b><math>88.71 \pm 0.19</math></b>
Our method	Cross-entropy loss	$86.57 \pm 0.21$

module, RVN-2, it performs a spatiotemporal convolution with  $3 \times 3 \times 3$  kernels and a temporal convolution with  $3 \times 1 \times 1$  kernels. And the third relation module named RVN-3 uses  $1 \times 3 \times 3$  convolution kernels in both convolution layers which only does spatial convolution. Under the 5-way 1-shot setting, the results on the UCF101 dataset are listed in Table 1. The accuracy of RVN-1 gains 2.5% and 3.46% improvements over RVN-2 and RVN-3 respectively for the 5-way 1-shot learning task. The results reflect the importance of modeling spatiotemporal information simultaneously.

**Different structures of LSTM.** In RVN, the video-level features of the support videos and query videos are obtained by averaging over the  $T$  clip-level feature maps, in which temporal ordering information is lost. Therefore, we propose to use long shot-term memory to model the long-term temporal information of  $T$  clips. We explore the influence of different structures of LSTM in Table 2. As mentioned in Section 3.2, the dimension of the embedded clip-level features is  $(C, T', H, W)$ . Using the convolutional layers of MFNet as the embedding layer,  $C, T', H,$  and  $W$  equal 768, 8, 4, and 4, respectively. To prevent overfitting, we use global average pooling to reduce the spatiotemporal dimension from  $(8, 4, 4)$  to  $(1, 1, 1)$  before feeding forward into LSTM. Therefore, the input dimension of LSTM is  $C=768$ . The corresponding results of different numbers of the units in hidden layer are listed in Table 2. Relatively, high dimensional features are more effective for sequence modeling and semantic alignment when comparing video-level similarities in few-shot action recognition. In addition, the results in Table 2 show that long-term temporal information is essential for few-shot action recognition compared with the results in Table 1.

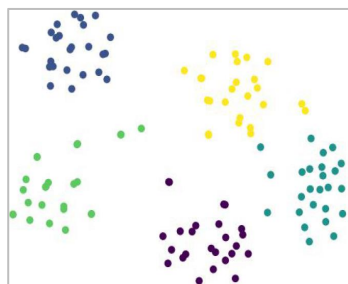
**Influence of circle loss.** In the pair similarity optimization module, we use circle loss to optimize our model. In order to prove that circle loss is a more effective optimization method, we compare it with cross-entropy loss (CEL) in this part. The performance with 5-way 1-shot setting on the UCF101 dataset is shown in Table 3. When using circle loss to optimize our model, the accuracy reaches  $88.71 \pm 0.19\%$ , which is 2.14% higher and with a more compact confidence interval than that



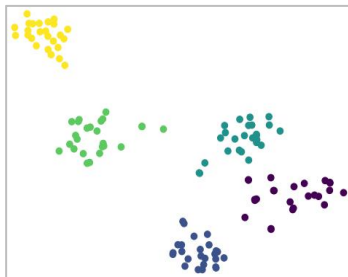
**Table 4**

Few-shot action recognition results. The mean accuracies of the 5-way 1-shot and 5-shot tasks on UCF101 and HMDB51 datasets are listed, with 95% confidence intervals.

Model	5-Way Accuracy (%)			
	UCF101		HMDB51	
	1-shot	5-shot	1-shot	5-shot
Generative Approach (Mishra et al., 2018)	-	78.68 ± 1.80	-	52.58 ± 3.10
Feature-Aligning Network (FAN) (Tan and Yang, 2019)	71.80 ± 0.10	86.50 ± 0.20	50.20 ± 0.20	67.60 ± 0.10
ProtoGAN (Kumar Dwivedi et al., 2019)	61.70 ± 1.60	79.70 ± 0.80	34.40 ± 1.30	50.90 ± 0.60
Action Relation Network (ARN) (Zhang et al., 2020)	62.10 ± 1.00	84.80 ± 0.80	44.60 ± 0.90	59.10 ± 0.80
<b>Our Method</b>	<b>88.71 ± 0.19</b>	<b>96.78 ± 0.08</b>	<b>63.43 ± 0.28</b>	<b>79.69 ± 0.20</b>



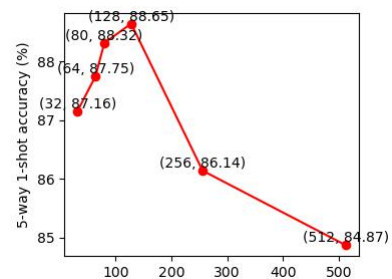
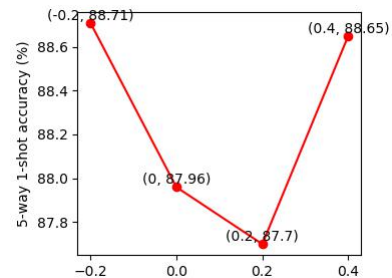
(a) Cross-entropy loss.



(b) Circle loss.

**Fig. 6 .** The t-SNE visualization (Maaten and Hinton, 2008) of the  $\mathcal{A}(\cdot)$  feature. (a) corresponds to the 5-way 1-shot setting of our model using CEL and (b) corresponds to our model using the circle loss. We can see that circle loss makes clusters more compact and discriminative from each other.

of CEL. As can be seen, with the circle loss, our model can perform better than the case of using the CEL. In addition, in order to observe the effects of CEL and circle loss on the features, we visualize the feature distribution of 5-way 1-shot setting using t-SNE (Maaten and Hinton, 2008) in Fig. 6. Compared with CEL, circle loss makes clusters more compact and discriminative from each other. In Fig. 7, we analyze the impact of the two hyperparameters for circle loss, *i.e.*, the scale factor  $\gamma$  and the relaxation factor  $m$ . We set  $\gamma$  to be 32, 64, 80, 128, 256, and 512 in Fig. 7 (a) with a fixed value of  $m$ , where  $m = 0.4$ . As can be seen, when  $\gamma$  varies between 32 and 128, circle loss surpasses CEL and has good robustness. Then we set  $\gamma$  to be 128 and vary  $m$  from -0.2 to 0.4 (with 0.2 as the interval) and visualize the results in Fig. 7 (b). Under these settings, circle

(a) scale factor  $\gamma$ .(b) relaxation factor  $m$ .

**Fig. 7 .** Impact of the two hyperparameters. (a) shows the accuracies corresponding to different values of the scale factor  $\gamma$ , and (b) shows the accuracies corresponding to different values of the relaxation factor  $m$  with 5-way 1-shot setting on UCF101 dataset.

loss surpasses the performance of CEL ( $86.57 \pm 0.21\%$ ) consistently.

#### 4.3.3. Evaluating Few-Shot Learning

We compare our proposed approach with other few-shot action recognition methods in this section. By default, we conduct 5-way few-shot action recognition. The 1-shot and 5-shot action recognition results on both the UCF101 and HMDB51 datasets are listed in Table 4. It can be observed that our method compares favorably against other methods by a large margin, not limited to the metric-based methods but also including the augmentation-based methods. Compared with ARN (Zhang et al., 2020), the performance is 88.71% vs 62.10%, 96.78%

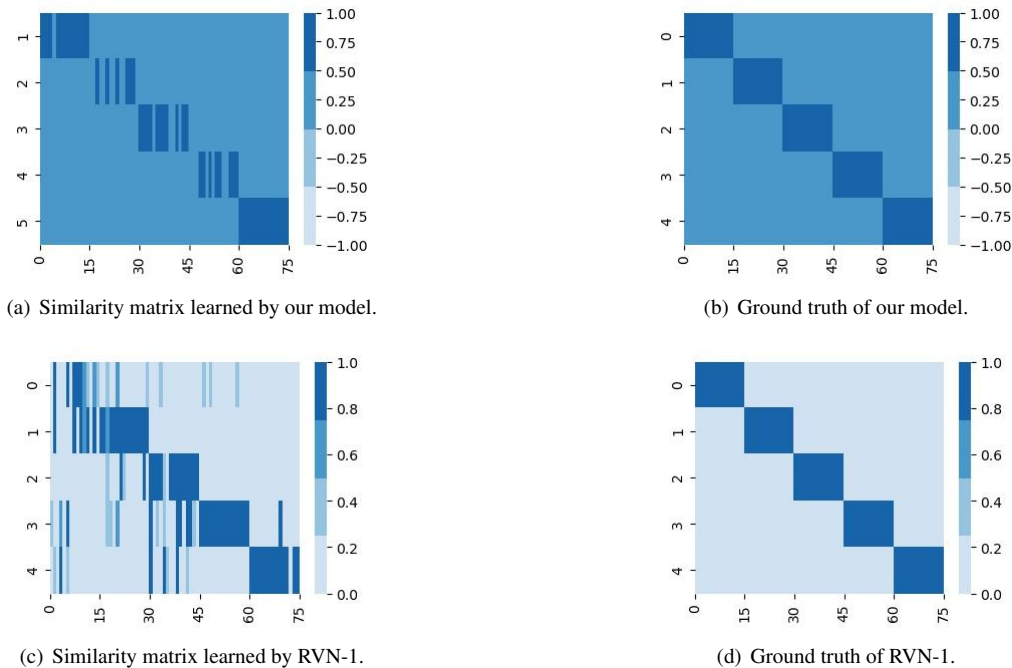


**Fig. 8 .** Similarity matrices learned by our proposed model, the baseline RVN-1, and the ground truth on UCF101 dataset under the 5-way 1-shot learning setting. Vertical axis denotes the index of the five classes in the support set. Horizontal axis denotes the index of the  $15 \times 5$  query videos.

vs. 84.80%, 63.43% vs. 44.60%, and 79.69% vs. 59.10% under 5-way 1-shot and 5-way 5-shot settings on the two benchmarks UCF101 and HMDB51, respectively. Compared with FAN (Tan and Yang, 2019), our method gains 16.91%, 10.28%, 13.23%, and 12.09% improvements on 5-way 1-shot and 5-way 5-shot action recognition tasks on UCF101 and HMDB51 datasets, respectively. By comparing with the competing methods, we could conclude that considering long-term temporal information, aligning video sequences implicitly, and allowing each similarity score to learn at its own pace help to enhance the generalization ability of the model on unseen classes for few-shot action recognition.

#### 4.3.4. Visualization

We visualize the similarity matrices learned by our proposed model with the implicit alignment and pair similarity optimization modules, and the baseline RVN-1 under the 5-way 1-shot learning setting on UCF101 dataset. We select 15 query videos from each class (*i.e.*, 75 query videos in total), calculate the similarity between each query video and the support video in each class, and visualize the  $5 \times 75$  similarity matrices. Note that the ground truth similarity scores for circle loss are different from those for CEL as introduced in Section 3.4. From Fig. 8, it can be seen that the similarity scores learned by our proposed model are much closer to the ground truth than those learned by the baseline model, which demonstrates the superior learning ability of our propose modules for few-shot action recognition.

## 5. Conclusion

In this paper, we propose a novel few-shot action recognition model. It aligns video sequences implicitly with long short-term memory units following 3D convolutional layers for sequence comparison, and adjusts the gradients on the video-level similarity scores dynamically during training for a more flexible and better optimization process. In addition, we present a standard and unambiguous experimental setting for performance evaluation. Extensive experiments verify the superiority of our method, which can handle the problem of semantic misalignment and wide variation in videos well with extremely limited data and achieve state-of-the-art accuracy on few-shot action recognition.

## Declaration of Competing Interest

The authors declare that they have no known competing financial interests or personal relationships that could have appeared to influence the work reported in this paper.

## Acknowledgments

This work is supported by the National Natural Science Foundation of China under Grant 61906155 and U19B2037, the Natural Science Foundation of Shaanxi Province under Grant 2020JQ-216, the China Postdoctoral Science Foundation under Grant 2020M673488, the Fundamental Research Funds for the Central Universities under Grant 31020180QD138, and the Open Projects Program of National Laboratory of Pattern Recognition.

## References

- Baik, S., Hong, S., Lee, K.M., 2020. Learning to forget for meta-learning, in: Proceedings of the IEEE/CVF Conference on Computer Vision and Pattern Recognition, pp. 2379–2387.
- Bilen, H., Fernando, B., Gavves, E., Vedaldi, A., Gould, S., 2016. Dynamic image networks for action recognition, in: Proceedings of the IEEE Conference on Computer Vision and Pattern Recognition, pp. 3034–3042.
- Bishay, M., Zoumpourlis, G., Patras, I., 2019. TARN: temporal attentive relation network for few-shot and zero-shot action recognition, in: 30th British Machine Vision Conference 2019, BMVC 2019, Cardiff, UK, September 9–12, 2019, BMVA Press. p. 154.
- Bo, Y., Lu, Y., He, W., 2020. Few-shot learning of video action recognition only based on video contents, in: The IEEE Winter Conference on Applications of Computer Vision, pp. 595–604.
- Bottou, L., 2010. Large-scale machine learning with stochastic gradient descent, in: Proceedings of COMPSTAT'2010. Springer, pp. 177–186.
- Cao, K., Ji, J., Cao, Z., Chang, C.Y., Niebles, J.C., 2020. Few-shot video classification via temporal alignment, in: Proceedings of the IEEE/CVF Conference on Computer Vision and Pattern Recognition, pp. 10618–10627.
- Chen, W., Liu, Y., Kira, Z., Wang, Y.F., Huang, J., 2019. A closer look at few-shot classification, in: International Conference on Learning Representations.
- Chen, Y., Kalantidis, Y., Li, J., Yan, S., Feng, J., 2018. Multi-fiber networks for video recognition, in: Proceedings of the European conference on computer vision (ECCV), pp. 352–367.
- Coskun, H., Zia, Z., Tekin, B., Bogo, F., Navab, N., Tombari, F., Sawhney, H., 2019. Domain-Specific Priors and Meta Learning for Low-shot First-Person Action Recognition. arXiv preprint arXiv:1907.09382 .
- Finn, C., Abbeel, P., Levine, S., 2017. Model-agnostic meta-learning for fast adaptation of deep networks, in: Proceedings of the 34th International Conference on Machine Learning-Volume 70, JMLR. org. pp. 1126–1135.
- Gidaris, S., Bursuc, A., Komodakis, N., Pérez, P., Cord, M., 2019. Boosting few-shot visual learning with self-supervision, in: Proceedings of the IEEE International Conference on Computer Vision, pp. 8059–8068.
- Guo, M., Chou, E., Huang, D.A., Song, S., Yeung, S., Fei-Fei, L., 2018. Neural graph matching networks for fewshot 3d action recognition, in: Proceedings of the European conference on computer vision (ECCV), pp. 653–669.
- Hao, F., He, F., Cheng, J., Wang, L., Cao, J., Tao, D., 2019. Collect and select: Semantic alignment metric learning for few-shot learning, in: Proceedings of the IEEE International Conference on Computer Vision, pp. 8460–8469.
- Hochreiter, S., Schmidhuber, J., 1997. Long short-term memory. Neural computation 9, 1735–1780.
- Hoffer, E., Ailon, N., 2015. Deep metric learning using triplet network, in: International Workshop on Similarity-Based Pattern Recognition, Springer. pp. 84–92.
- Huang, H., Zhang, J., Zhang, J., Wu, Q., Xu, J., 2019. Compare more nuanced: Pairwise alignment bilinear network for few-shot fine-grained learning, in: 2019 IEEE International Conference on Multimedia and Expo (ICME), IEEE. pp. 91–96.
- Kay, W., Carreira, J., Simonyan, K., Zhang, B., Hillier, C., Vijayanarasimhan, S., Viola, F., Green, T., Back, T., Natsev, P., et al., 2017. The kinetics human action video dataset. arXiv preprint arXiv:1705.06950 .
- Koch, G., Zemel, R., Salakhutdinov, R., 2015. Siamese neural networks for one-shot image recognition, in: ICML deep learning workshop.
- Kuehne, H., Jhuang, H., Garrote, E., Poggio, T., Serre, T., 2011. Hmdb: a large video database for human motion recognition, in: 2011 International Conference on Computer Vision, IEEE. pp. 2556–2563.
- Kumar Dwivedi, S., Gupta, V., Mitra, R., Ahmed, S., Jain, A., 2019. ProtoGAN: Towards Few Shot Learning for Action Recognition, in: Proceedings of the IEEE International Conference on Computer Vision Workshops, pp. 1308–1316.
- Li, H., Dong, W., Mei, X., Ma, C., Huang, F., Hu, B.G., 2019a. Lgm-net: Learning to generate matching networks for few-shot learning, in: International conference on machine learning, pp. 3825–3834.
- Li, W., Wang, L., Xu, J., Huo, J., Gao, Y., Luo, J., 2019b. Revisiting local descriptor based image-to-class measure for few-shot learning, in: Proceedings of the IEEE Conference on Computer Vision and Pattern Recognition, pp. 7260–7268.
- Lifchitz, Y., Avrithis, Y., Picard, S., Bursuc, A., 2019. Dense classification and implanting for few-shot learning, in: Proceedings of the IEEE Conference on Computer Vision and Pattern Recognition, pp. 9258–9267.
- Maaten, L.v.d., Hinton, G., 2008. Visualizing data using t-sne. Journal of machine learning research 9, 2579–2605.
- Mishra, A., Verma, V.K., Reddy, M.S.K., Arulkumar, S., Rai, P., Mittal, A., 2018. A generative approach to zero-shot and few-shot action recognition, in: 2018 IEEE Winter Conference on Applications of Computer Vision (WACV), IEEE. pp. 372–380.
- Müller, M., 2007. Dynamic time warping. Information retrieval for music and motion , 69–84.
- Murphy, K.P., 2012. Machine learning: a probabilistic perspective. MIT press.
- Oreshkin, B., López, P.R., Lacoste, A., 2018. Tadam: Task dependent adaptive metric for improved few-shot learning, in: Advances in Neural Information Processing Systems, pp. 721–731.
- Paszke, A., Gross, S., Chintala, S., Chanan, G., Yang, E., DeVito, Z., Lin, Z., Desmaison, A., Antiga, L., Lerer, A., 2017. Automatic differentiation in pytorch. 31st Conference on Neural Information Processing Systems (NIPS 2017) .
- Ravi, S., Larochelle, H., 2017. Optimization as a model for few-shot learning, in: International Conference on Learning Representations.
- Snell, J., Swersky, K., Zemel, R., 2017. Prototypical networks for few-shot learning, in: Advances in Neural Information Processing Systems, pp. 4077–4087.
- Soomro, K., Zamir, A.R., Shah, M., 2012. Ucf101: A dataset of 101 human actions classes from videos in the wild. arXiv preprint arXiv:1212.0402 .
- Sun, Y., Cheng, C., Zhang, Y., Zhang, C., Zheng, L., Wang, Z., Wei, Y., 2020. Circle loss: A unified perspective of pair similarity optimization, in: Proceedings of the IEEE/CVF Conference on Computer Vision and Pattern Recognition, pp. 6398–6407.
- Sung, F., Yang, Y., Zhang, L., Xiang, T., Torr, P.H., Hospedales, T.M., 2018. Learning to compare: Relation network for few-shot learning, in: Proceedings of the IEEE Conference on Computer Vision and Pattern Recognition, pp. 1199–1208.
- Tan, S., Yang, R., 2019. Learning similarity: Feature-aligning network for few-shot action recognition, in: 2019 International Joint Conference on Neural Networks (IJCNN), IEEE. pp. 1–7.
- Vinyals, O., Blundell, C., Lillicrap, T., Wierstra, D., et al., 2016. Matching networks for one shot learning, in: Advances in neural information processing systems, pp. 3630–3638.
- Xian, Y., Sharma, S., Schiele, B., Akata, Z., 2019. f-vaegan-d2: A feature generating framework for any-shot learning, in: Proceedings of the IEEE Conference on Computer Vision and Pattern Recognition, pp. 10275–10284.
- Zhang, H., Zhang, J., Koniusz, P., 2019. Few-shot learning via saliency-guided hallucination of samples, in: Proceedings of the IEEE Conference on Computer Vision and Pattern Recognition, pp. 2770–2779.
- Zhang, H., Zhang, L., Qui, X., Li, H., Torr, P.H., Koniusz, P., 2020. Few-shot action recognition with permutation-invariant attention, in: Proceedings of the European Conference on Computer Vision (ECCV).
- Zhu, L., Yang, Y., 2018. Compound memory networks for few-shot video classification, in: Proceedings of the European Conference on Computer Vision (ECCV), pp. 751–766.

## Supplementary Material

### *The splitting setting of the UCF101 dataset.*

*Training classes of the UCF101 data:* MilitaryParade, JavelinThrow, Biking, Drumming, SoccerJuggling, Haircut, Typing, FrontCrawl, FrisbeeCatch, Kayaking, WritingOnBoard, LongJump, BandMarching, HulaHoop, CricketBowling, PullUps, JumpingJack, BodyWeightSquats, Mixing, Basketball, Rafting, ShavingBeard, RopeClimbing, Hammering, Fencing, Archery, TrampolineJumping, ApplyEyeMakeup, BalanceBeam, TableTennisShot, Lunges, PlayingCello, JugglingBalls, HeadMassage, Knitting, BasketballDunk, Swing, PizzaTossing, WallPushups, BlowDryHair, TaiChi, Billiards, FieldHockeyPenalty, Nunchucks, BabyCrawling, Ski-jet, SumoWrestling, BrushingTeeth, PoleVault, BoxingPunchingBag, PlayingViolin, YoYo, BenchPress, PlayingDhol, UnevenBars, Rowing, Bowling, MoppingFloor, PushUps, Soc-

cerPenalty, PlayingFlute, PlayingTabla, BaseballPitch, PlayingPiano, WalkingWithDog, PlayingSitar, BreastStroke, BoxingSpeedBag, ParallelBars, ThrowDiscus.

*Validation classes of the UCF101 data:* ApplyLipstick, HammerThrow, Shotput, HighJump, HandstandPushups, SkateBoarding, CricketShot, HorseRiding, PlayingDaf, PlayingGuitar.

*Test classes of the UCF101 data:* BlowingCandles, RockClimbingIndoor, PommelHorse, HorseRace, Skiing, HandstandWalking, JumpRope, CleanAndJerk, CliffDiving, VolleyballSpiking, Surfing, Diving, StillRings, SalsaSpin, FloorGymnastics, Punch, GolfSwing, IceDancing, CuttingInKitchen, TennisSwing, SkyDiving.

*The splitting setting of the HMDB51 dataset.*

*Training classes of the HMDB51 data:* shoot bow, climb, hug, catch, clap, pullup, wave, throw, dribble, ride bike, sword, kiss, fall floor, punch, jump, chew, shake hands, situp, brush hair, stand, turn, dive, flic flac, drink, handstand, climb stairs, sword exercise, ride horse, draw sword, push, walk.

*Validation classes of the HMDB51 data:* laugh, golf, smile, cartwheel, swing baseball, somersault, shoot gun, shoot ball, hit, eat.

*Test classes of the HMDB51 data:* pushup, kick ball, pick, run, kick, talk, sit, smoke, fencing, pour.